This article has been accepted for publication in a future issue of this journal, but has not been fully edited. Content may change prior to final publication. Citation information: DOI 10.1109/TAP.2018.2829824, IEEE Transactions on Antennas and Propagation

Millimeter-Wave Wideband Circularly Polarized Planar Complementary Source Antenna with End-Fire Radiation

Jingxue Wang, Yujian Li, *Member*, *IEEE*, Lei Ge, *Member*, *IEEE*, Junhong Wang, *Senior Member*, *IEEE*, Meie Chen, Zhan Zhang, and Zheng Li, *Member, IEEE*

***Abstract*—A novel circularly polarized (CP) complementary source antenna with end-fire radiation is proposed in Ka-band. With the existence of two antipodal notches etched at the edges of the two broad walls of an open-ended substrate integrated waveguide (SIW), two orthogonal electric field components radiated from the equivalent magnetic current and the electric currents separately can be excited simultaneously. The magnitude and phase differences between the two filed components can be controlled effectively by properly tuning the dimensions of the notches. The operating mechanism and the design procedure of the antenna are analyzed in detail. Wide -10 dB impedance and 3-dB axial ratio (AR) bandwidths of 64% and 51%, a gain varying from 3.1 to 6.4 dBic, and the symmetrical radiation pattern are obtained. In order to further increase the gain and front to back ratio (FTBR) of the antenna, a dielectric rod structure is then integrated with the antenna. An overlapped operating bandwidth of 41%, an improved gain up to 12 dBic and the stable radiation pattern with an FTBR close to 20 dB are verified by a fabricated prototype. The antenna presented in this paper provides a new mean to design the wideband end-fire CP antenna with a simple configuration, which would be attractive for future millimeter-wave wireless systems.**

***Index Terms*—Complementary source antenna, circularly polarization, end-fire radiation, the fifth generation (5G) mobile communications, millimeter waves.**

I. Introduction

CIRCULARLY polarized (CP) antennas have been widely adopted in modern wireless communication systems for decades due to their superior properties of reducing the polarization mismatch and the multipath distortion [1]. The most commonly used idea to realize the CP antenna is to excite two orthogonal operating modes with similar magnitudes and a 90° phase difference in a radiating element [2]. Various types of the CP antennas based on this method have been developed, including the crossed dipole [3], the microstrip patch antenna [4], [5], the slot antenna [6] and the dielectric resonator antenna (DRA) [7], [8]. Because of the same operating mechanism and neighboring resonant frequencies of the two excited modes, the sizes of these CP antennas should be similar to each other in two orthogonal dimensions. Therefore, they are suitable for the applications requiring broadside CP radiation, but not desirable for the planar antenna or array design with end-fire CP radiation, which are highly demanded by some low-profile wireless devices operating in microwave and millimeter-wave bands [9]. In order to overcome the issue, several planar antenna designs with the end-fire CP characteristics, such as the planar helical antenna [10], the antipodal linearly tapered slot antenna (ALTSA) [11]-[13], the substrate integrated sloping slot loaded horn antenna [14], and the antenna using combined magnetic dipoles [9], [15], have been investigated in the literature, where 3-dB axial ratio bandwidths up to 35% have been achieved.

As a sort of the wideband radiating elements, the antenna consisting of the complementary source, i.e. the combination of the electric and magnetic currents, have attracted increasing attention in the last decade [16]-[20]. By employing an electric dipole and an equivalent magnetic dipole arranged in orthogonal directions with an in-phase excitation, linearly polarized broadside radiation can be implemented by the magneto-electric (ME) dipole antenna originally revealed in [16]. The CP radiation has been generated by a dual-feed ME-dipole fed by a feed network which can realize the 90° phase difference [17]. After that, a single-feed wideband CP aperture-coupled ME-dipole antenna was reported in [18] as well. More recently, the concept of the ME-dipole antenna has been extended to the antenna design with end-fire radiation [19], [20]. Wide bandwidth and good radiation performance can be achieved, but all these designs are still linearly polarized.

Actually, by feeding an electric dipole and an equivalent magnetic dipole that are parallel to each other with similar magnitudes and a 90° phase difference, another kind of the complementary source antenna with unidirectional CP radiation properties can be implemented. The idea was first demonstrated in designing CP antennas with broadside radiations by applying a slot antenna integrated with various parasitic dipole structures [21]-[24]. However, due to its narrow configuration caused by the parallel electric and magnetic dipoles, this kind of the complementary source antenna may find more advantages in the design of the planar end-fire CP antennas. Very recently, a few designs following this method have been addressed [25]-[28]. An open-ended substrate integrated waveguide (SIW) cavity [25] or a

Manuscript received by *, 2017. This work was supported in part by the National Natural Science Foundation of China under Grant No. 61671052, the National Nature Science Foundation of China under Grant 61331002 and the National Nature Science Foundation of China under Grant 61571039.

J. X. Wang, Y. J. Li, J. H. Wang, M. E. Chen, Z. Zhang and Z. Li are with the Institute of Lightwave Technology, Beijing Jiaotong University, Beijing 100044, China (Corresponding author e-mail: liyujian@bjtu.edu.cn).

L. Ge is with the College of Electronic Science and Technology, Shenzhen University, Shenzhen, China. (E-mail: leige@szu.edu.cn).

This article has been accepted for publication in a future issue of this journal, but has not been fully edited. Content may change prior to final publication. Citation information: DOI 10.1109/TAP.2018.2829824, IEEE Transactions on Antennas and Propagation

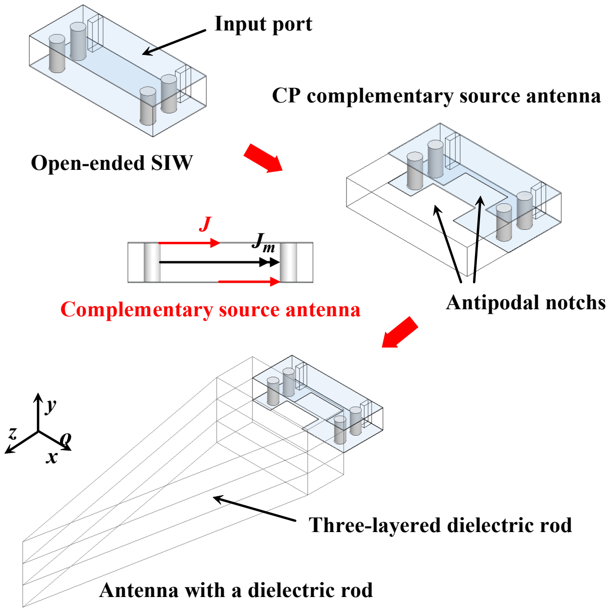

Fig. 1. Design procedure of the proposed antenna with end-fire CP radiation.

quarter-wavelength shorted patch [26], [27] was employed as the equivalent magnetic dipole, while an additional electric dipole [25]-[27] was arranged in front of the magnetic dipole with a small distance. For the purpose of realizing the required 90° phase difference, a short section of the straight or meander parallel line was used as the delay line for linking the magnetic and the electric dipoles [25], [27]. The end-fire CP radiation has been verified, but the impedance or 3-dB axial ratio (AR) bandwidth was narrower than 5%. Furthermore, the Yagi-Uda array has also been introduced in [28] to enhance the bandwidth and gain characteristics of this kind of complementary source antenna. Nevertheless, the operating bandwidth of the design was only around 10% yet.

In this paper, a novel complementary source antenna with end-fire CP radiation features is presented in Ka-band. Different from most previous works, wide impedance and AR bandwidths of greater than 40% can be fulfilled successfully, while the entire design still maintains a simple and compact planar configuration. Furthermore, in order to further improve the gain and front to back ratio (FTBR) performance, a dielectric rod that was used in a linearly polarized antenna [29] is loaded in front of the CP complementary source antenna. Stable radiation patterns with low backward radiation and high gain can be achieved successfully. Due to its compact geometry, wide operating band, and desirable radiation properties, it is believed that the proposed CP antenna can found possible applications in future millimeter-wave wireless applications, including the fifth-generation (5G) mobile communications and the next generation WiFi systems.

The paper is organized as follows. Section II illustrates the antenna geometry. Section III depicts the operating mechanism and the detailed design procedure of the antenna. Measured results and discussions are presented in Section IV and Section V gives a final conclusion.

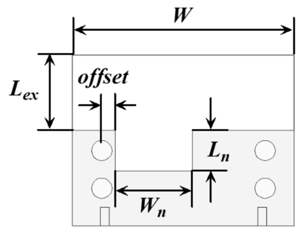

Fig. 2. Top view of the proposed CP antenna with detailed dimensions.

TABLE I
DIMENSIONS OF THE PROPOSED CP ANTENNA (UNITS: mm)

Parameters	W	W_n	L_n	L_{ex}	*offset*
Values	7.6	2.65	1.4	2.6	0.45

II. ANTENNA CONFIGURATION

Design process of the proposed antenna illustrated in Fig. 1 starts from an open-ended SIW section, whose radiation is similar to a magnetic dipole since the electric filed over the radiating aperture can be seen as a magnetic current J_m in horizontal direction shown in Fig. 1 [19]. In order to realize the CP complementary source antenna, two antipodal notches are cut at the edges of the broad walls of the open-ended SIW. It is well known that the electric currents on the left and right half of broad walls of a rectangular waveguide are out of phase. Therefore, by removing the two sections on the broad walls at antipodal positions, the electric currents J on the remaining portions of the broad walls are in phase as indicated in Fig. 1, and thus operate as an electric dipole in horizontal direction. As will be discussed in Section III-B, the magnitude and phase differences between J and J_m can be adjusted effectively by varying the dimensions of the notches properly. As a result, CP radiation at the end-fire direction can be expected when the similar magnitudes and the 90° phase difference between the complementary sources are satisfied. Additionally, as illustrated in Fig. 1, the substrate in front of the radiating aperture is extended outward for obtaining better impedance matching [19] and AR performance.

Theoretically, the CP complementary source antenna would generate a donut-shaped omnidirectional radiation pattern. However, for millimeter-wave applications, the directional radiation with high gain is desirable for the purpose of compensating the large propagation loss in free space. In this work, a dielectric rod consisting of three substrate layers is introduced, which will be confirm in Section III-C that it is a promising mean to increase the gain and FTBR of the CP end-fire antenna.

III. ANTENNA DESIGN

The top view of the CP complementary source antenna with detailed dimensions is shown in Fig. 2, where the length and width of the notch are L_n and W_n, respectively. Rogers 5880 printed circuit board (PCB) laminates with a relative dielectric constant of 2.2 and a thickness of 1.575 mm are applied in this paper [30]. The width of the feeding SIW is 5.6 mm to ensure

This article has been accepted for publication in a future issue of this journal, but has not been fully edited. Content may change prior to final publication. Citation information: DOI 10.1109/TAP.2018.2829824, IEEE Transactions on Antennas and Propagation

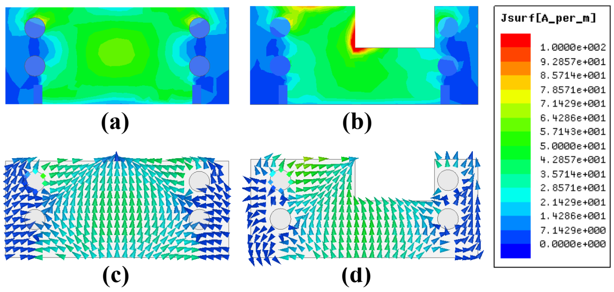

Fig. 3. Simulated electric field distributions on the broad wall of the open-ended SIW without (a), (c) and with (b), (d) the notch. (a), (b) magnitude distributions, (c), (d) vector distributions.

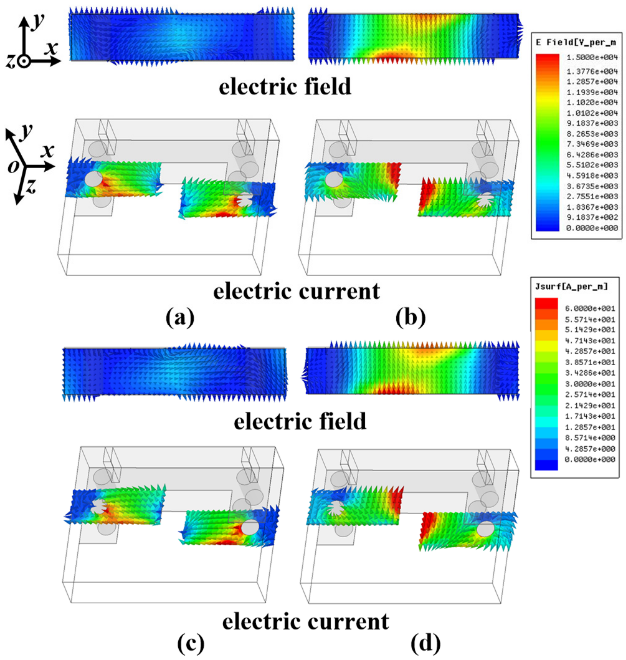

Fig. 4. Simulated electric field and current distributions of the proposed antenna in a period. (a) $t = 0$, (b) $t = T / 4$, (c) $t = T / 2$, (d) $t = 3T / 4$.

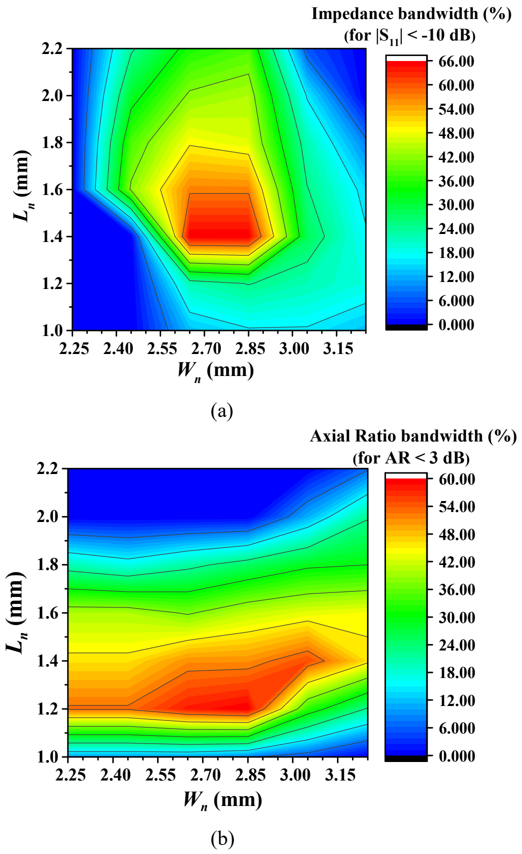

Fig. 5. Simulated bandwidth of the CP antenna with different values of L_n and W_n. (a) Impedance bandwidth for $|S_{11}| < -10$ dB, (b) Axial ratio bandwidth for AR < 3 dB.

only the TE_{10} mode is excited over the frequency band of interest from 19.8 to 39.6 GHz. The diameter and period of the vias are set to be 0.7 mm and 1.3 mm respectively to prevent the undesirable leakage based on the design guideline of the SIW given in [31]. By fine tuning the dimensions of the antenna, the final values of the parameters are listed in Table I

A. Operating Principle

For the purpose of revealing the operating mechanism of the proposed antenna, the simulated electric current distributions on one of the broad walls is provided in Fig. 3, where the magnitude and vector distributions for the antenna without the notches are exhibited in (a) and (c), while the counterpart for the design with the notches are given in (b) and (d). Two conclusions can be seen by comparing the results. First, the electric current distribution on the broad wall is not affected remarkably by the existence of the notch, which means that electric field distribution within the open-ended SIW with notches is similar to that when there is no notch. Second, considering the 180° phase difference between the electric currents on the top and bottom broad walls, the currents on the remaining portion of the edges of the two broad walls are in same orientation by adding the two antipodal notches. Therefore, the currents can combine together to operate as an electric dipole.

Simulated electric field over the SIW aperture behind the notches and the currents on the remaining portions of the broad walls are then illustrated in Fig. 4 to demonstrate the CP features of the proposed antenna. As shown in Fig. 4 (a), the electric field across the SIW aperture is very weak, but the electric currents on the remaining portion of the broad walls are strong and the component directing to right orientation is dominant, which verifying that the electric current $\boldsymbol{J}$ is excited effectively at $t = 0$. On the other hand, the electric field across the SIW aperture is strong at $t = T / 4$, where T is a period of time. Although the currents on the top and bottom broad walls are strong yet, their directions are opposite and thus the radiation fields would be cancelled mutually. It means that only the magnetic current $\boldsymbol{J}_m$ is excited at the moment. The filed and current distributions at $t = T / 2$ and t = $3T / 4$ are same with those at $t = 0$ and t = $T / 4$ but the directions are opposite. As a summary, the electric and magnetic currents can be excited alternatively with a 90° phase difference in this antenna. The radiation fields generated by the two kinds of currents also have similar magnitudes as will be shown in the next section. Therefore, the CP radiation field at the end-fire direction can be realized by the proposed complementary source antenna.

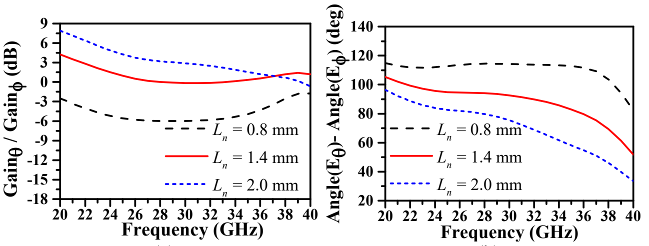

(a) (b)

Fig. 6. Effects of L_n on the radiation fields of the proposed CP antenna. (a) The magnitude difference between E_h and E_v, (b) The phase difference between E_h and E_v.

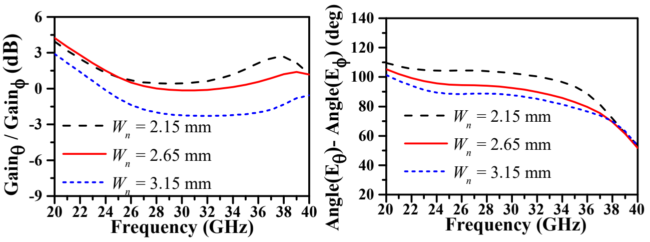

(a) (b)

Fig. 7. Effects of W_n on the radiation fields of the proposed CP antenna. (a) The magnitude difference between E_h and E_v, (b) The phase difference between E_h and E_v.

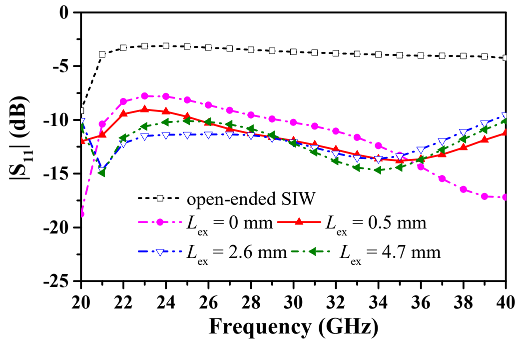

Fig. 8. Simulated $|S_{11}|$ of the CP antenna with varying values of L_{ex}.

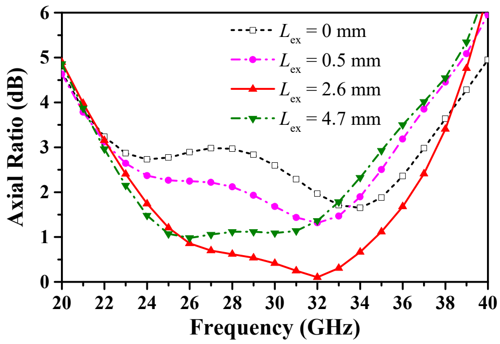

Fig. 9. Simulated AR of the CP antenna with varying values of L_{ex}.

B. Design of the CP Complementary Source Antenna

It is found in the studies that the magnitude and the phase of the complementary currents can be tuned significantly with the length L_n and the width W_n of the notches, so a parametric study on the two parameters is implemented as illustrated in Fig. 5 to explore the design rules of the antenna. L_n and W_n vary from 1 to 2.2 mm and from 2.25 to 3.25 mm, respectively. Other parameters unmentioned are kept same with those given in Table I. Clearly, the influences of the two parameters on the impedance bandwidth for $|S_{11}| < -10$ dB and the 3-dB AR bandwidth are different. The variation of the impedance bandwidth follows an approximately radial distribution, while the variation of the 3-dB AR bandwidth is mainly controlled by L_n. By comparing the results shown in Fig. 5 (a) and (b), it can be found that the widest overlapped operating bandwidth of around 50% occurs when L_n is close to 1.4 mm and W_n is in the vicinity of 2.75 mm.

For better understanding the physical insight of the CP radiation properties of the antenna, the simulated relationship between the two orthogonal radiation field components in the end-fire direction (*z*-axis in Fig. 1), i.e. the electric field in horizontal direction (*xoz*-plane in Fig. 1) E_h and the electric filed in vertical direction (*yoz*-plane in Fig. 1) E_v, for different L_n and W_n is presented in Fig. 6 and Fig. 7, respectively. Values of other parameters are same with those in Table I.

It can be observed in Fig. 6 (a) that the ratio of E_h to E_v increases with L_n and approaches 0 dB throughout a wide frequency range when L_n equals to 1.4 mm. As mentioned in Section II, the antipodal notches can excite the radiation from the electric currents on the broad walls by removing the currents with opposite orientation. Hence, a larger L_n means more currents causing cancellation in radiation can be removed such that stronger E_h is obtained. However, it should be noted that persistent increase in L_n cannot lead to consistent enhancement in E_h because the electric currents in reversed direction would exist on the broad wall as indicated in Fig. 3. On the other hand, L_n is related to the path difference between the two complementary sources, namely the electric currents on the remaining portions of the broad walls and the magnetic current lying on the aperture behind the notches, and thus it is able to control the phase difference between E_h and E_v as depicted in Fig. 6 (b). The required 90° phase difference can be achieved within a wide frequency band when L_n is close to 1.4 mm as well. Therefore, good AR performance can be realized as aforementioned in Fig. 5 (b).

As shown in Fig. 7 (a), the ratio of E_h to E_v decreases slightly for W_n varying from 2.15 to 3.15 mm, which can be attributed to that portion of the electric currents on the broad walls with a same direction begins to be removed as well when W_n is larger than half of the SIW width. Furthermore, the phase difference between E_h and E_v is not affected by the variation of W_n significantly as illustrated in Fig. 7 (b). Actually, the two requirements for realizing CP radiation can be obtained simultaneously when W_n is around half of the SIW width, and this is why the AR bandwidth given in Fig. 5 (b) is not sensitive to W_n. However, it is found in studies that a too small or large value of W_n is not acceptable for getting good CP properties.

The extended substrate with a length of L_{ex} in front of the radiating aperture of the CP antenna is employed as a method to fine tune the impedance matching characteristics in this work. Fig. 8 illustrates the simulated $|S_{11}|$ of the open-ended SIW without notches and the proposed CP antenna with different values of L_{ex}. The open-ended SIW suffers from a poor

This article has been accepted for publication in a future issue of this journal, but has not been fully edited. Content may change prior to final publication. Citation information: DOI 10.1109/TAP.2018.2829824, IEEE Transactions on Antennas and Propagation

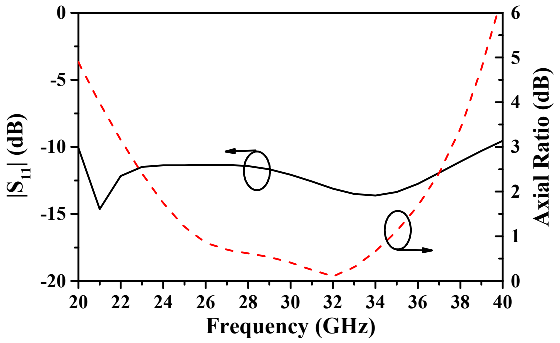

Fig. 10. Simulated $|S_{11}|$ and AR of the proposed CP complementary source antenna.

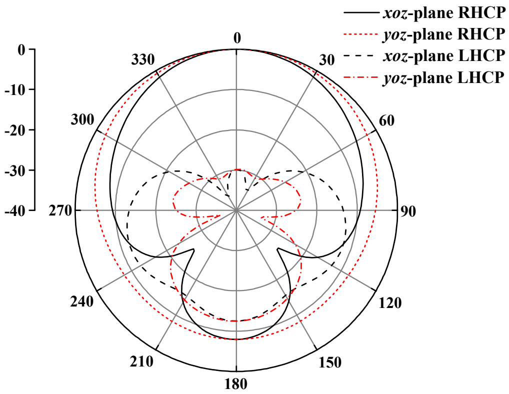

Fig. 11. Simulated radiation patterns of the proposed CP complementary source antenna at 30 GHz.

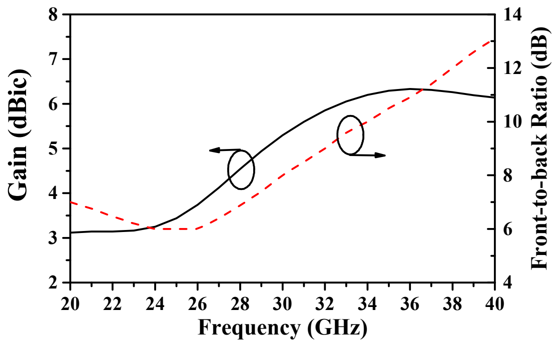

Fig. 12. Simulated gain and FTBR of the proposed CP complementary source antenna.

impedance matching. By loading the two antipodal notches, $|S_{11}|$ of the antenna is improved but is slightly higher than -10 dB yet over the major portion of the frequency range. Then, by extending the substrate and adjusting its length, a wide band can be achieved for $|S_{11}|$ < -10 dB, which confirms the effectiveness of this approach.

The simulated AR results of the antenna for different values of L_{ex} are presented in Fig. 9. It is seen that although the AR performance can be influenced by L_{ex} slightly, its value maintains below than 3 dB throughout the major portion of the frequency range when L_{ex} is changed. Therefore, promising impedance and AR bandwidths can be realized simultaneously by properly adjusting L_{ex}.

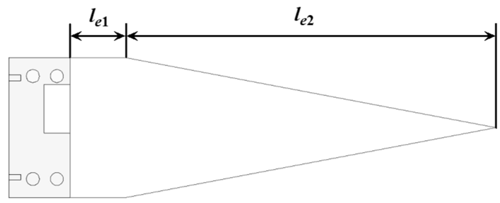

Fig. 13. Top view of the proposed CP antenna loaded with the dielectric rod.

According to the above analysis, the simulated results of the proposed CP complementary source antenna can be obtained. The simulated impedance bandwidth for $|S_{11}|$ < -10 dB and the 3-dB AR bandwidth are 64.2% (from 20.2 to 39.3 GHz) and 51.4% (from 22.1 to 37.4 GHz) separately as indicated in Fig. 10, which demonstrates that the overlapped operating bandwidth of the proposed CP antenna is larger than 50%. The simulated radiation pattern of the proposed antenna at 30 GHz is presented in Fig. 11. The radiation pattern is symmetrical and directs to the end-fire direction. Besides, it has a wide 3-dB AR beamwidth of around 120° in the *xoz*-plane and 240° in the *yoz*-plane. As shown in Fig. 12, the antenna has a gain varying from 3.1 to 6.4 dBic and an FTBR of larger than 6 dB across the entire operating band, which are comparable with the performance of reported planar end-fire CP antenna designs in [9], [15], and [25]-[27].

C. Design of the Antenna with a Dielectric Rod

Wide operating bandwidth and satisfying radiation features have been obtained in Section III-B. In this section, the gain and FTBR of the proposed end-fire CP complementary source antenna will be further improved in order to meet some millimeter-wave applications with the high-gain requirement. Specifically, a three-layered dielectric rod implemented in PCB laminates is introduced in front of the radiating aperture of the antenna as illustrated in Fig. 13, whose length is controlled by two parameters l_{e1} and l_{e2}. The width of the dielectric rod keeps the same with that of the antenna and then is linearly tapered in *xoz*-plane for the purpose of obtaining better impedance transformation between the substrate and the air and also enhancing the radiation in end-fire direction. For ease of realization, the middle Rogers 5880 PCB laminate is extended forward and two extra PCB laminates with the same shape and thickness are attached on the top and bottom surfaces of the middle layer by using adhesive. The effect of the parameters l_{e1} and l_{e2} on the properties of the antenna will be investigated here in detail. The original values of l_{e1} and l_{e2} are set to 3 and 20 mm, respectively. Other dimensions of the antenna keep the same values listed in Table I.

By comparing the simulated results of the CP antennas with different values of l_{e1} and l_{e2} that are given in Fig. 14 and Fig. 15, it can be seen that both of the two parameters do not affect $|S_{11}|$ of the antenna significantly. Additionally, the simulated gain and FTBR are almost unchanged for different l_{e1}, but are improved obviously by increasing l_{e2}. When l_{e1} = 3 mm and l_{e2} = 20 mm, the gain of the antenna is from 9 to 13 dBic and the FTBR is greater than 12 dB over the entire operating band, which verifies that an improvement of 6 dB in both the gain and FTBR can be achieved with the existence of the dielectric rod.

This article has been accepted for publication in a future issue of this journal, but has not been fully edited. Content may change prior to final publication. Citation information: DOI 10.1109/TAP.2018.2829824, IEEE Transactions on Antennas and Propagation

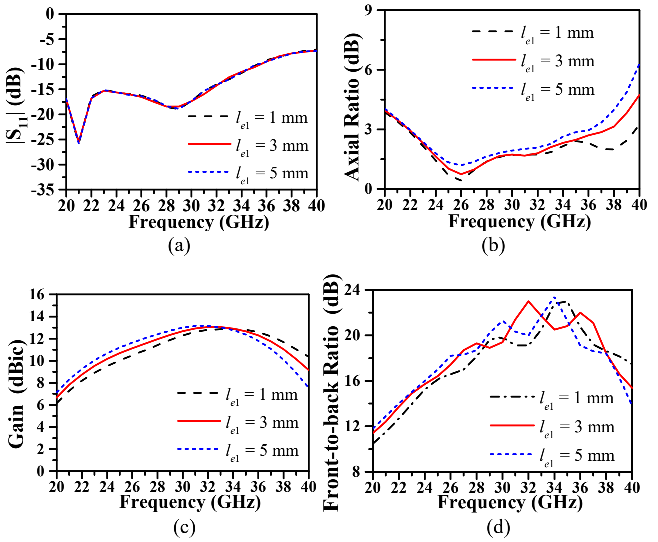

Fig. 14. Effects of l_{e1} on the proposed CP antenna. (a) $|S_{11}|$. (b) AR. (c) Gain. (d) FTBR.

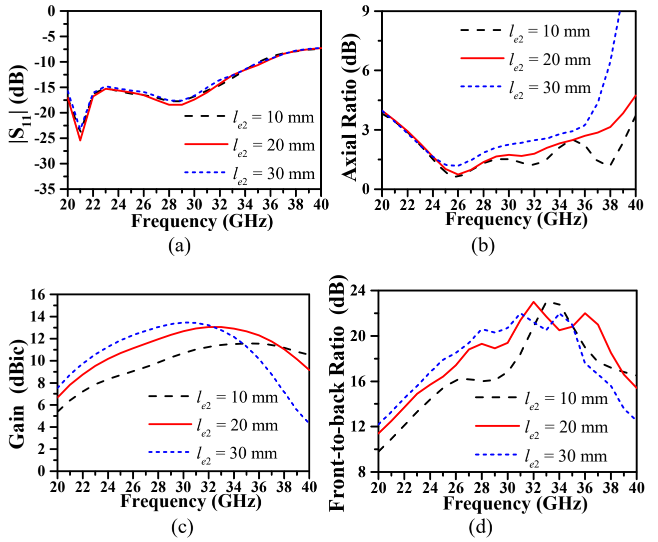

Fig. 15. Effects of l_{e2} on the proposed CP antenna. (a) $|S_{11}|$. (b) AR. (c) Gain. (d) FTBR.

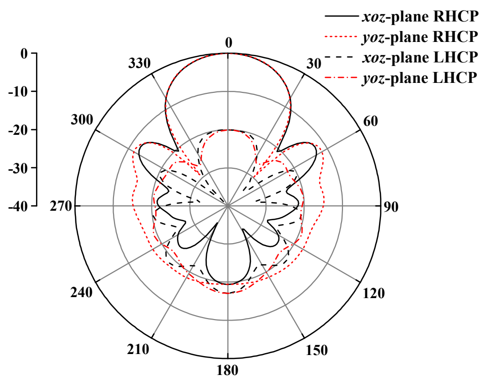

Fig. 16. Simulated radiation patterns of the antenna loaded with dielectric rod at 30 GHz.

However, as indicated in Fig. 15, further increase in l_{e2} will degrade the radiation characteristics of the antenna at high-end of the operating band. Therefore, 3 and 20 mm are finally selected as the values of l_{e1} and l_{e2} in the antenna design.

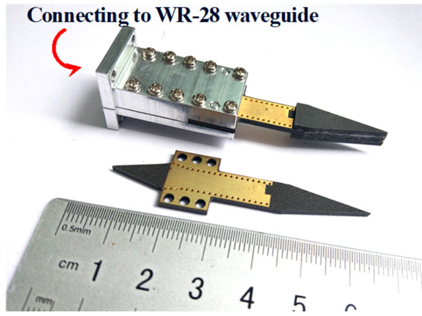

Fig. 17. Photograph of the fabricated prototypes of the planar end-fire CP antennas with an SIW to waveguide transition.

The simulated radiation pattern of the CP antenna loaded with the dielectric rod at 30 GHz is presented in Fig. 16. Clearly, the beamwidth in both the *xoz*- and *yoz*- planes is narrowed in comparison with the counterpart shown in Fig. 11. Moreover, the backward radiation is reduced apparently. The sidelobes appearing at around ±50º are mainly caused by the loaded dielectric rod.

D. Design Guideline

Based on the above studies, a design guideline of the proposed CP complementary source antenna is summarized as below.

1) The dimensions of the open-ended SIW are determined first by taking account of the frequency of interest.

2) Add two antipodal notches at the edges of the SIW broad walls separately. The initial values of the length and width of the notches can be set to a quarter of the operating wavelength in the substrate at the center frequency and half of the width of the SIW, respectively. Properly adjust the dimensions of the notches to get promising antenna performance.

3) Introduce the tapered dielectric rod in front of the antenna. Gradually increase the length of the rod to achieve the improved gain and FTBR properties.

IV. Measurement and Discussion

The proposed CP planar complementary source antenna loaded with the tapered dielectric rod was fabricated and measured to verify the design as presented in Fig. 17. For the sake of measurement, a wideband SIW to WR-28 waveguide transition initially reported in [32] is integrated at the input port of the antenna. The feeding SIW is extended backward to diminish the effect of the aluminum transition. An Agilent Network Analyzer E8363C was used for testing the matching properties of the antenna. The far-field radiation characteristics of were performed in an anechoic chamber. The gain of the antenna was obtained by comparing with a CP standard gain horn with an operating band from 29 to 34 GHz, while the AR is calculated by comparing the maximum with the minimum received power of a rotated linearly polarized horn.

A. Measured Results

Measured and simulated $|S_{11}|$ of the antenna are given in Fig. 18. The measured impedance bandwidth for $|S_{11}| < -10$ dB is 52.9% (from 22.5 to 38.7 GHz). It is seen that the measured results and the simulated results with the aluminum fixture are in better agreement, which indicates the effect of the fixture.

This article has been accepted for publication in a future issue of this journal, but has not been fully edited. Content may change prior to final publication. Citation information: DOI 10.1109/TAP.2018.2829824, IEEE Transactions on Antennas and Propagation

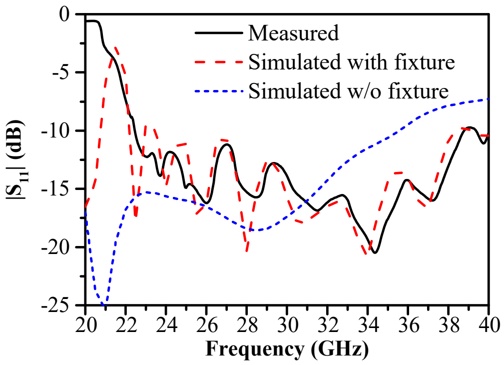

Fig. 18. Measured and simulated $|S_{11}|$ of the proposed CP antenna.

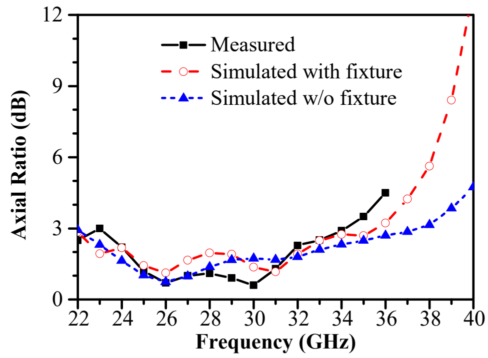

Fig. 19. Measured and simulated AR of the proposed CP antenna.

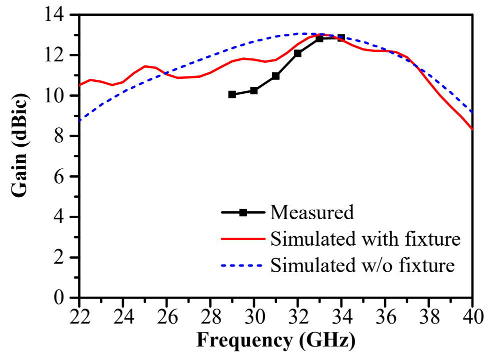

Fig. 20. Measured and simulated gain of the proposed CP antenna.

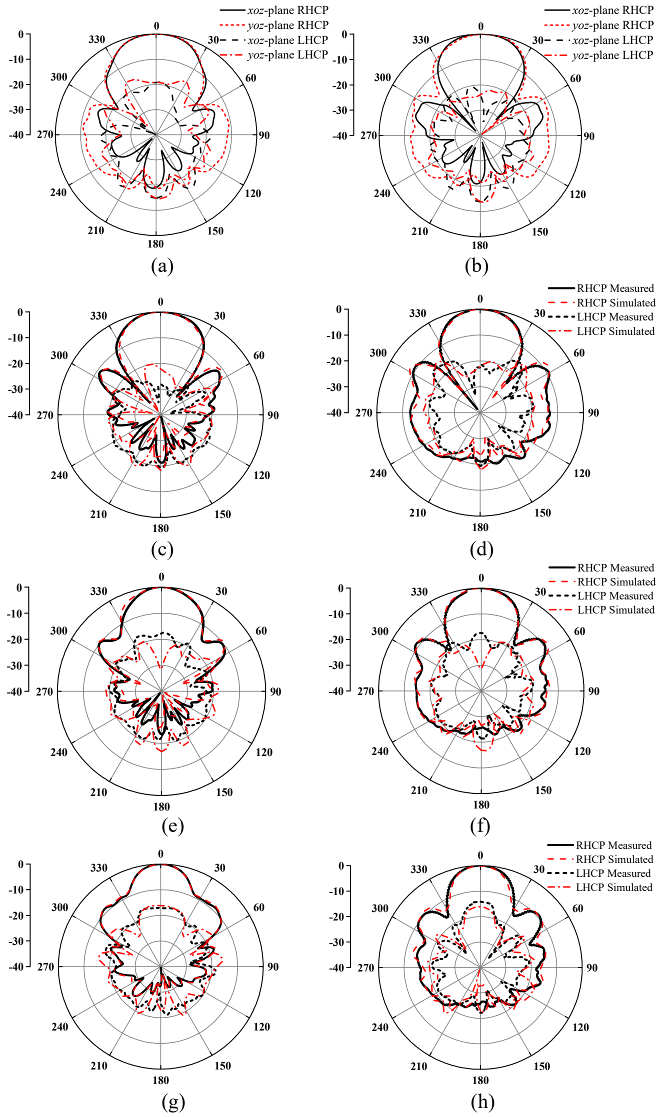

Fig. 21. Measured and simulated radiation patterns of the proposed CP antenna. (a) simulated results at 23 GHz, (b) simulated results at 26 GHz, (c) *xoz*-plane at 30 GHz, (d) *yoz*-plane at 30 GHz, (e) *xoz*-plane at 32 GHz, (f) *yoz*-plane at 32 GHz, (g) *xoz*-plane at 34 GHz, (h) *yoz*-plane at 34 GHz.

Fig. 19 depicts the measured and simulated AR of the antenna at end-fire direction. A wide measured 3-dB AR bandwidth of 43% (from 22 to 34 GHz) is achieved. Additionally, it is observed that the measured AR is slightly larger than the simulated one when frequency is higher than 33 GHz. In order to reveal the possible reason for this discrepancy, the simulated AR obtained from the antenna model with the aluminum fixture is also provided in Fig. 19, where a better agreement between the simulated and measured results can be seen. Therefore, similar to the $|S_{11}|$ results, the slight difference in AR at high-end frequencies can be mainly attributed to the influence of the fixture although the feeding SIW has been extended. By comparing the results of $|S_{11}|$ and AR, it can be found that an overlapped operating band of 41% (from 22.5 to 34 GHz) can be achieved by the proposed antenna.

Fig. 20 presents the measured and simulated gain of the fabricated antenna. Due to the limited operating band of the CP standard gain horn available in the laboratory, the measured results are obtained only within the frequency range between 29 GHz and 34 GHz. The measured gain varies from 10.1 to 12.9 dBic, which is slightly lower than the simulated results. The small difference would result from the alignment tolerance and the possible effect from the measurement setup.

Measured and simulated radiation patterns of the fabricated antenna at 30, 32 and 34 GHz are depicted in Fig. 21, where good agreement is obtained. The radiation patterns are symmetrical in both the *xoz*- and *yoz*- planes and the measured FTBR of the antenna is around 20 dB. Furthermore, the simulated radiation patterns of the antenna with the fixture at lower frequencies are illustrated in Fig. 21 (a) and (b) as well. The simulated radiation patterns in the diagonal planes at 30 GHz are presented in Fig. 22 (a) and (b). The cross polarization level is lower than -19 dB, which means that the CP radiation properties are maintained.

This article has been accepted for publication in a future issue of this journal, but has not been fully edited. Content may change prior to final publication. Citation information: DOI 10.1109/TAP.2018.2829824, IEEE Transactions on Antennas and Propagation

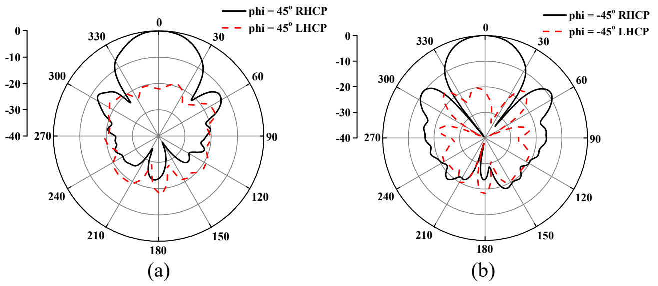

Fig. 22. Simulated radiation patterns of the antenna with fixture at diagonal planes. (a) φ =45° plane at 30 GHz, (b) φ = -45° plane at 30 GHz.

TABLE II
COMPARISON BETWEEN PROPOSED AND REPORTED END-FIRE CP ANTENNAS

Ref.	Type	Geometry Features	Imp. BW (-10 dB)	3-dB AR BW	Max. Gain (dBic)
[9]	Combined magnetic dipoles	Planar PCB	2.4%	9.2%	2.6
[15]	Combined magnetic dipoles	Planar PCB	22.2%	8%	2
[10]	Helical antenna	Planar PCB	54%	34%	10.5
[11]	Tapered slot	Metallic structure	35%	35%	12.6
[12]	Tapered slot	Metallic structure	40%	34%	11
[25]	Complementary dipoles	Planar PCB	2%	14.5%	2.3
[28]	Complementary dipoles	Planar PCB	13.1%	10.5%	8.2
This work	Complementary dipoles	Planar PCB	64.2%	51.4%	6.4
This work	Complementary dipoles (with a dielectric rod)	Planar PCB	52.9%	41%	12.9

B. Comparison and Discussion

The configuration features and the main performance of different types of the end-fire CP antennas reported in the literature are summarized in Table II for comparison with this work.

In terms of the antenna geometries, most designs are realized by applying the planar PCB facilities, which have advantages of ease of integration and low fabrication costs, except the two tapered slot antennas [11], [12]. Compared with the tapered slot antennas and the planar helical antenna presented in [10], [11] and [12], all the reported CP end-fire antennas consisting of two magnetics dipoles or the complementary dipoles suffer from narrow overlapped operating bands of around or less than 10%. Benefiting the novel configurations proposed in this paper, the achievable impedance and CP bandwidths of the end-fire complementary source antenna can be improved significantly, which are even better than the counterparts of the tapered slot and planar helical antennas. On the other hand, the gain of the CP end-fire complementary source antennas, including the designs in [25], [28] and this paper, is relatively low in comparison with the tapered slot and planar helical antennas, due to their omnidirectional radiation features in theory. In this work, by employing the loaded dielectric rod, an obvious increase in gain is also obtained successfully. The maximum gain of 12.9 dBic of the proposed antenna is comparable with the previous designs with high-gain characteristics.

V. CONCLUSION

A novel millimeter-wave wideband circularly polarized planar complementary source antenna with end-fire radiation has been presented. Two antipodal notches etched at the edges of the broad walls of an open-ended substrate integrated waveguide have been utilized to produce the radiation from the electric currents. A tapered dielectric rod implemented in three substrate layers is added to further improve the gain and the front to back ratio of the antenna. The operating principle and design considerations have been investigated in detail. A wide overlapped operating bandwidth of larger than 40% has been demonstrated by a fabricated prototype. Meanwhile, the proposed antenna also have stable gain of around 11.5 dBic and symmetrical end-fire radiation patterns with a front to back ratio of close to 20 dB. Because of advantages of excellent operating characteristics, a simple configuration, and ease of fabrication, the proposed circularly polarized end-fire antenna would be a promising candidate for future wideband and multi-band millimeter-wave wireless applications.

REFERENCES

[1] Steven Gao, Qi Luo, and Fuguo Zhu, *Circularly polarized antennas*, John Wiley & Sons, 2014.
[2] Warren L. Stutzman, and Gary A. Thiele, *Antenna theory and design*, John Wiley & Sons, 2012.
[3] J. Baik, K. J. Lee, W. S. Yoon, T. H. Lee, and Y. S. Kim, “Circularly polarised printed crossed dipole antennas with broadband axial ratio,” *Electron. Lett.*, vol. 44, no. 13, pp. 785–786, Jun. 2008.
[4] H. Wong et al., “Small antennas in wireless communications,” *Proc. IEEE*, vol. 100, no. 7, pp. 2109–2121, Jul. 2012.
[5] T. Nakamura and T. Fukusako, “Broadband design of circularly polarized microstrip patch antenna using artificial ground structure with rectangular unit cells,” *IEEE Trans. Antennas Propag.*, vol. 59, no. 6, pp. 2103–2010, Jun. 2011.
[6] K. Ding, C. Gao, T. Yu, and D. Qu, “Wideband CP slot antenna with backed FSS reflector,” *IET Microwave, Antennas and Propagation*, vol. 11, no. 7, pp. 1045-1050, Jul. 2017.
[7] K. M. Luk and K. W. Leung, *Dielectric Resonator Antennas*. Baldock, U.K.: Research Studies Press, 2003.
[8] Y. Pan and K. W. Leung, “Wideband circularly polarized trapezoidal dielectric resonator antenna,” *IEEE Antennas Wireless Propag. Lett.*, vol. 9, pp. 588–591, 2010.
[9] W.-J. Lu, J.-W. Shi, K.-F. Tong, and H.-B. Zhu, “Planar endfire circularly polarized antenna using combined magnetic dipoles,” *IEEE Antennas Wireless Propag. Lett.*, vol. 14, pp. 1263–1266, 2015.
[10] Z. Chen and Z. Shen, “Planar helical antenna of circular polarization,” *IEEE Trans. Antennas Propag.*, vol. 63, no. 10, pp. 4315–4323, Oct. 2015.
[11] Y. Liu, H. Lu, Y. Wu, M. Cui, B. Li, P. Zhao, and X. Lv, “Millimeterwave and Terahertz Waveguide-Fed Circularly Polarized Antipodal Curvedly Tapered Slot Antennas,” *IEEE Trans. Antennas Propag.*, vol. 64, no. 5, pp. 1607–1614, May 2016.
[12] Y. Yao, X. Cheng, J. Yu, and X. Chen, “Analysis and Design of a Novel Circularly Polarized Antipodal Linearly Tapered Slot Antenna,” *IEEE Trans. Antennas Propag.*, vol. 64, no. 10, pp. 4178–4187, Oct. 2016.
[13] L. Wang, X. Yin, M. Esquius-Morote, H. Zhao, and J. R. Mosig, “Circularly Polarized Compact LTSA Array in SIW Technology,” *IEEE Trans. Antennas Propag.*, vol. 65, no. 6, pp. 3247–3252, Jun. 2017.
[14] Y. Cai, Y. Zhang, Z. Qian, W. Cao, and S. Shi, “Compact Wideband Dual Circularly Polarized Substrate Integrated Waveguide Horn Antenna,” *IEEE Trans. Antennas Propag.*, vol. 64, no. 7, pp. 3184–3189, Jul. 2016.

This article has been accepted for publication in a future issue of this journal, but has not been fully edited. Content may change prior to final publication. Citation information: DOI 10.1109/TAP.2018.2829824, IEEE Transactions on Antennas and Propagation

[15] M. You, W.-J. Lu, B. Xue, L. Zhu, and H.-B. Zhu, “A novel planar endfire circularly polarized antenna with wide axial-ratio beamwidth and wide impedance bandwidth,” *IEEE Trans. Antennas Propag.*, vol. 64, no. 10, pp. 4554–4559, Oct. 2016.

[16] K. M. Luk and H. Wong, “A new wideband unidirectional antenna element,” *Int. J. Microw. Opt. Technol*., vol. 1, no. 1, pp. 35–44, Jun. 2006.

[17] K. Mak and K. Luk, “A circularly polarized antenna with wide axial ratio beamwidth,” *IEEE Trans. Antennas Propag.*, vol. 57, no. 10, pp. 3309–3312, Oct. 2009.

[18] Y. J. Li and K. M. Luk, “A 60-GHz wideband circularly polarized aperture-coupled magneto-electric dipole antenna array,” *IEEE Trans. Antennas Propag.*, vol. 64, no. 4, pp. 1325–1333, Apr. 2016.

[19] Y. J. Li and K. M. Luk, “A multibeam end-fire magnetoelectric dipole antenna array for millimeter-wave applications,” *IEEE Trans. Antennas Propag.*, vol. 64, no. 7, pp. 2894–2904, Jul. 2016.

[20] J. X. Wang, Y. J. Li, L. Ge, J. H. Wang, M. E. Chen, Z. Zhang, and Z. Li, “Wideband Dipole Array Loaded Substrate Integrated H-plane Horn Antenna for Millimeter Waves,” *IEEE Trans. Antennas Propag.*, Accepted for publication, 2017.

[21] X. Bai, S.-W. Qu, and K. B. Ng, “Millimeter-wave cavity-backed patchslot dipole for circularly polarized radiation,” *IEEE Antennas Wireless Propag. Lett.*, vol. 12, pp. 1355–1358, 2013.

[22] M. Li and K. M. Luk, “A wideband circularly polarized antenna for microwave and millimeter-wave applications,” *IEEE Trans. Antennas Propag.*, vol. 62, no. 4, pp. 1872–1879, Apr. 2014.

[23] Q. Zhu, K.-B. Ng, C. H. Chan, “Printed Circularly Polarized Spiral Antenna Array for Millimeter-Wave Applications,” *IEEE Trans. Antennas Propag.*, vol. 65, no. 2, pp. 636–643, Feb. 2017.

[24] X. Ruan, S.-W. Qu, Q. Zhu, K. B. Ng, and C. H. Chan, “A Complementary Circularly Polarized Antenna for 60-GHz Applications,” *IEEE AntennasWireless Propag. Lett.*, vol. 16, pp. 1373–1376, 2017.

[25] W.-H. Zhang, W.-J. Lu, and K.-W. Tam, “A planar end-fire circularly polarized complementary antenna with beam in parallel with its plane,” *IEEE Trans. Antennas Propag.*, vol. 64, no. 3, pp. 1146–1152, Mar. 2016.

[26] J. Liu, Y. Li, Z. Liang, and Y. Long, “A planar quasi-magnetic–electric circularly polarized antenna,” *IEEE Trans. Antennas Propag.*, vol. 64, no. 6, pp. 2108–2114, Jun. 2016.

[27] M. Ye, X.-R. Li, and Q.–X. Chu, “Single layer circularly polarized antenna with fan-beam endfire radiation,” *IEEE Antennas and Wireless Propag. Lett.*, vol. 16, pp. 20–23, 2017.

[28] W. L. Zhou, J. H. Liu and Y. L. Long, “A broadband and high-gain planar complementary yagi array antenna with circular polarization,” *IEEE Trans. Antennas Propag.*, vol. 65, no. 3, pp.1446–1451, Mar. 2017.

[29] C. Prasad, and A. Biswas, “Planar excitation of dielectric waveguide antenna for broadband and high-gain application,” *IEEE Antennas and Wireless Propag. Lett.*, vol. 16, pp. 1209–1212, 2017.

[30] RT/duroid 5880® High Frequency Laminates. Ansoft Corp., Canonsburg, Rogers Corp., USA [Online]. Available: http://www.rogerscorp.com/documents/606/acs/RT-duroid-5870-5880-Data-Sheet.pdf

[31] D. Deslandes and K. Wu, “Accurate modeling, wave mechanisms, and design considerations of a substrate integrated waveguide,” *IEEE Trans. Microw. Theory Tech.*, vol. 54, no. 6, pp. 2516–2526, Jun. 2006.

[32] D. Dousset, K. Wu, and S. Claude, “Millimeter-wave broadband transition of substrate-integrated waveguide to rectangular waveguide,” *Electron. Lett.*, vol. 46, no. 24, pp. 1610–1611, Nov. 2010.

Jingxue Wang was born in Jilin, China. She received the B.Eng degree in electrical engineering from Beijing Jiaotong University, Beijing, China, in 2015 and is currently working towards the Ph.D. degree in electrical engineering at the same university.

Her research interests focus on millimeter wave antennas and arrays.

Miss Wang received the Best Student Paper Awards at UCMMT 2016 and ACES 2017.

Yujian Li (S’12–M’15) was born in Hunan, China, in 1987. He received the B.S. and M.S. degrees in communications engineering from Beijing Jiaotong University, Beijing, China, in 2009 and 2012, respectively, and the Ph.D. degree in electronic engineering from City University of Hong Kong in 2015.

He joined the Institute of Lightwave Technology at Beijing Jiaotong University in 2015 as an Associate Professor. His current research interests include millimeter wave antennas, base station antennas and leaky wave structures.

Dr. Li was awarded the Outstanding Research Thesis Award from City University of Hong Kong in 2015. He received the Best Paper Award at the 2015 IEEE Asia-Pacific Conference on Antennas and Propagation (APCAP), the Best Student Paper at 2013 National Conference on Antennas, and the Best Student Paper Award (2nd Prize) at the 2013 IEEE International Workshop on Electromagnetics (iWEM). He was selected as a Finalist in the student paper contest of 2015 IEEE AP-S Symposium on Antennas and Propagation (APS). He has served as a Reviewer for the IEEE Transactions on Antennas and Propagation, the IEEE Antennas and Wireless Propagation Letters, and the IET Microwaves, Antennas & Propagation.

JunhongWang (M’02–SM’03) was born in Jiangsu, China, in 1965. He received the B.S. and M.S. degrees in electrical engineering from the University of Electronic Science and Technology of China, Chengdu, China, in 1988 and 1991, respectively, and the Ph.D. degree in electrical engineering from Southwest Jiaotong University, Chengdu, China, in 1994. In 1995, he joined as the Faculty with the Department of Electrical Engineering, Beijing Jiaotong University, Beijing, China, where he became a Professor in 1999. From January 1999 to June 2000, he was a Research Associate with the Department of Electric Engineering, City University of Hong Kong, Kowloon Tong, Hong Kong. From July 2002 to July 2003, he was a Research Scientist with Temasek Laboratories, National University of Singapore, Singapore. He is currently with the Key Laboratory of all Optical Network and Advanced Telecommunication Network, Ministry of Education of China, Beijing Jiaotong Univeristy, Beijing, China, and also with the Institute of Lightwave Technology, Beijing Jiaotong University, Beijing, China. His research interests include numerical methods, antennas, scattering, and leaky wave structures.

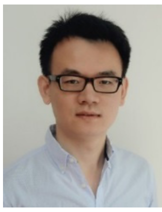

Lei Ge (S’11–M’15) was born in Jiangsu, China. He received the B.S. degree in electronic engineering from Nanjing University of Science and Technology, Nanjing, China, in 2009 and the Ph.D. degree in electronic engineering from City University of Hong Kong, Hong Kong, in 2015. From September 2010 to July 2011, he was a Research Assistant with the City University of Hong Kong. From April 2015 to October 2015, he was a Postdoctoral Research Fellow at the State Key Laboratory of Millimeter Waves, City University of Hong Kong. He is currently Assistant Professor and Associate Head of Department of Electronic Engineering at Shenzhen University, China.

He received the Honorable Mention at the student contest of 2012 IEEE APS-URSI Conference and Exhibition held in Chicago, US. He won the 1st Prize in the Student Innovation Competition of 2014 IEEE International Workshop on Electromagnetics (IEEE iWEM) held in Sapporo, Japan, in 2014. He was the Session Chair of the iWEM 2017 and ACES-China 2017. He was the TPC Member of the APCAP 2016. His recent research interest focuses on wideband antennas, patch antennas, base station antennas, reconfigurable antennas, the antennas for cognitive radio, and filtering antennas.

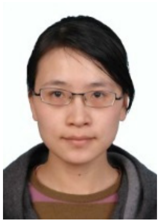

Meie Chen received the B.S. degree in Information and Tele-communication Engineering and Ph.D. degree in Electromagnetic and Microwave Technology from Beijing Jiaotong University, Beijing, China, in 2003 and 2009, respectively.

She is currently a lecture in the Institute of Lightwave Technology at Beijing Jiaotong University. Her research interests include antenna theory and technology, metasurface, RCS reduction technique.

Zhan Zhang received B.S degree in Electronics and Communications Engineering from Jilin University, China in 2002 and Ph.D. degree in electrical engineering from Nanyang Technological University, Singapore, in 2010. She joined the Faculty of School of Electronics and Information Engineering, Beijing Jiaotong University, Beijing, China, in 2010, where she is currently an associate professor. Her current research interests include metamaterial-based antenna design and transformation optics.

Zheng Li received the B.S. degree in physics and M.S. degree in electrical engineering from Beijing Jiaotong University, Beijing, China, in 2006 and 2012, respectively. From 2008 to 2009, he was a visiting student with the Pennsylvania State University, Pennsylvania, USA.

In 2012, he joined the faculty of the Department of Electrical Engineering, Beijing Jiaotong University, where he became an associate professor in 2015. His research interests include leaky-wave antennas and periodic structures.